Journal of Hydrology 616 (2023) 128852

Contents lists available at ScienceDirect

Journal of Hydrology

journal homepage: www.elsevier.com/locate/jhydrol

Research papers

+Dynamic identification and risk analysis of compound dry-hot events considering nonstationarity

Pengcheng Xu [a,b,*], Dong Wang [b,*], Yuankun Wang [c,*], Vijay P. Singh [d], Jianchun Qiu [a], Jichun Wu [b], Along Zhang [b], Xiaopei Ju [b]

[a] College of Hydraulic Science and Engineering, Yangzhou University, Yangzhou, PR China
[b] Key Laboratory of Surficial Geochemistry, Ministry of Education, Department of Hydrosciences, School of Earth Sciences and Engineering, State Key Laboratory of Pollution Control and Resource Reuse, Nanjing University, Nanjing, PR China
[c] School of Water Resources and Hydropower Engineering, North China Electric Power University, Beijing, PR China
[d] Department of Biological and Agricultural Engineering, Zachry Department of Civil & Environmental Engineering, Texas A & M University, College Station, TX77843, USA, and National Water and Energy Center, UAE University, Al Ain, United Arab Emirates

ARTICLE INFO

This manuscript was handled by Andras Bardossy, Editor-in-Chief, with the assistance of Ashish Sharma, Associate Editor

Keywords:
Compound dry-hot extremes
Dynamic copula
Nonstationarity
Risk
Multivariate

ABSTRACT

Duo to the influence of anthropogenic and climate change, the traditional drought or hot event identification indices under the stationary assumption of the probabilistic behavior of a hydrometeorological variable could be no longer valid. This study proposed a nonstationary framework for the identification of compound dry-hot extremes and risk assessment considering climate change for the warm season during the period 1901–2017 in Weihe River Basin (WRB) and Fenhe River Basin (FRB), China. The proposed framework is composed of three phases: (1) calculating nonstationary precipitation index (NSPI) and standardized temperature index (NSTI) by incorporating large-scale climate indices as covariates of fitted distribution parameters; (2) calculating nonstationary compound dry-hot index (NCDH) based on nonstationary copula models; and (3) bivariate nonstationary risk analysis of compound dry-hot events through two regional characteristics called relative affected area (*RA*) and mean severity of area (*MSA*). The proposed NCDH using climate indices as covariates was found to be superior in capturing compound dry-hot characteristics and revealing the trend of temporal and spatial changes of WRB over the period of 1901–2017. Based on the nonstationary risk assessment of regional characteristics, the occurrence risk of compound extremes in Sub-Basin 1 of WRB was less than that in the other two Sub-Basins. Considering the importance of nonstationarity during the above three modelling phases, the nonstationarity in the 1st phase modelling of average precipitation (AP) and average temperature (AT) to derive NSPI and NSTI could have a greater impact on the final results of nonstationary risk assessment of compound dry-hot events than nonstationarity in the other two phases. This nonstationary compound dry-hot index provides a new insight into compound extreme identification and risk assessment that can adapt to a changing environment.

1. Introduction

Frequencies and intensities of extreme events in the context of an anthropogenic warming climate, especially hot extremes and drought events, have experienced a substantial increase on a wide range of temporal and spatial scales all over the world (Zscheischler et al., 2018; Miralles et al., 2019; Alizadeh et al., 2020; Wang et al., 2020; Abatzoglou et al., 2021; Wang et al., 2021). Owing to the significantly adverse impacts triggered by these extreme events individually, the occurrence probabilities of hazardous states of one corresponding variable at a time have commonly been quantified by conventional climate risk analyses (Zscheischler and Seneviratne, 2017). The concurrence of extreme hydroclimatic events (i.e. compound dry-hot extremes) causes more disastrous impacts on agricultural productivity, human health, and ecosystem than does a single extreme event (Guerreiro et al., 2018). As a result, assessment of dynamic variations of compound dry and hot events is essential for determining potential driving forces which control the evolution of these concurrent events (Wu et al., 2020).

Systematic integration of climatic information from multiple related to the properties of these compound dry-hot events helps reflect their

* Corresponding authors at: College of Hydraulic Science and Engineering, Yangzhou University, Yangzhou, PR China (P. Xu).
E-mail addresses: m18994113495@163.com (P. Xu), wangdong@nju.edu.cn (D. Wang), yuankunw@ncepu.edu.cn, yuankunw@ncepu.edu.cn (Y. Wang).

https://doi.org/10.1016/j.jhydrol.2022.128852
Received 20 March 2022; Received in revised form 10 July 2022; Accepted 15 November 2022
Available online 26 November 2022

multivariate nature (Leonard et al., 2014). Much of the literature has quantitatively assessed the compound drought-heatwave events from two perspectives: (1) a certain threshold-based frequency variability assessment by extracting frequencies of concurrences of drought and hot extremes for the period of interest (Mazdiyasni and AghaKouchak, 2015; Miao et al.,2016; Zscheischler et al., 2018; Chen et al., 2019; Ribeiro et al., 2020); (2) a joint index covering multiple extremes or events which can quantify different properties, such as severity level and spatial extent for compound dry-hot extremes (Gallant et al., 2014; Wu et al., 2019; Wu et al., 2020; Hao et al., 2020). For instance, the Climate Extremes Index (CEI), proposed by Gallant et al. (2014), can be established by integrating multiple extremes with linear averaging of the areas covered by different extreme indicators.

In recent years, copulas, accounting for the dependence structure of multiple contributing variables, have been employed to measure the overall severity of compound droughts and hot extremes. For example, Hao et al. (2019, 2020) first proposed the Standardized Compound Event Indicator (SCEI) at a monthly scale to quantify the potential severity of compound dry-hot events by normalizing the joint cumulative probability of dry-hot events. Li et al. (2021) applied a daily-scale joint index, called the standardized compound drought and heat index (SCDHI), to quantify sub-monthly characteristics of compound dry and hot events and to monitor their initiation, development, and decay. With these above systematic joint indexes, the frequency, severity, duration, and intensity of compound dry-hot events can be quantified.

The above-mentioned joint indexes assessing the compound dry-hot events are all based on the underlying assumption that the hydrological processes and meteorological time series are stationary. As a result of anthropogenic greenhouse gas emissions, climate is changing, altering the composition of Earth's atmosphere, which has not only increased the complexity of hydrometeorological simulations, but has also necessitated the incorporation of nonstationarities in modelling hydrometeorological variables (Milly et al., 2008; Xiong et al., 2015; Blöschl et al., 2017; Kundzewicz et al., 2018; Xu et al., 2020a, 2020b). Therefore, recent literature has focused on nonstationarity of hydrometeorological variables caused by significant trend, abrupt changes or periodicity (Razmi et al., 2017; Salas and Obeysekera, 2014; Vasiliades et al., 2015; Zeng et al., 2017). For meteorological drought quantified by Standardized Precipitation Index (SPI), some researchers have applied nonstationary SPI (NSPI) to assess temporal variations of drought, which assume that the scale parameter of gamma distribution for SPI can change with time (Li et al., 2015; Park et al., 2019; Russo et al., 2013; Song et al., 2020). In the context of climate change, nonstationarity has been incorporated in not only drought analysis but also the hazard assessment of extreme precipitation and floods, in which the parameter set of potential best-fitted distribution exhibits a linear or nonlinear relation with time (Bender et al., 2014; Jiang et al., 2015; Rosner et al.,2014; Salas and Obeysekera, 2014; Sarhadi et al., 2016; Sarhadi and Soulis, 2017; Yan et al., 2017; Xu et al., 2020b) or some physical covariates (e.g. large-scale climate driving factors) (Agilan and Umamahesh, 2017; Liu et al.,2017; Gu et al., 2019; Razmi et al., 2017; Su and Chen, 2019; Vasiliades et al., 2015; Villarini et al., 2009; Xiong et al., 2015; Xu et al., 2020a; Yilmaz et al., 2017). Parallel to the potential nonstationarity existing in a drought index, it is essential to incorporate the nonstationary characteristics into the Standardized Compound Dry-Hot Event Indicator (CDH) monitoring the compound dry-hot conditions.

Several studies in China have focused on a systematic understanding of compound dry-hot events at different temporal and spatial scales (Chen et al., 2019; Hao et al., 2019; Wu et al., 2020; Zhang et al., 2019),. However, they have mostly focused on the frequency and severity of compound dry-hot events under stationary assumption, therefore it is necessary to apply the nonstationary CDH index to detect and monitor the compound dry-hot events with consideration of environmental changes.

The main objective of this study therefore was to develop a dynamic extreme joint index (nonstationary compound dry-hot event index, NCDH) for detecting compound droughts and hot extremes with the use of time-varying copula models (Sarhadi et al., 2016; Xu et al., 2020a, 2020b) accounting for the dependence of multiple variables. We also applied dynamic copula-based bivariate frequency analysis considering the severity and affected area of compound dry-hot events. These two properties (severity and area) of compound dry-hot events were extracted from the grid-based hydrometeorological dataset of Weihe River basin of China by the nonstationary monitoring index NCDH. Since there are teleconnections between larger-scale climate indices and drought or heatwaves in many regions across the world, climate indices were incorporated as covariates of NCDH.

2. Study area and dataset

Weihe River basin, which is located in northwest China (Fig. 1), embraces fragile ecological environment, and experiences frequent natural disasters. Compound dry-hot extreme events have posed a significant impact on the regional economic structure and the rational development and utilization of water resources. According to the water system distribution characteristics, the whole basin can be divided into three sub-basins: the main stream of the Weihe River (Sub-Basin 3 in Fig. 1), the Jinghe River basin (Sub-Basin 2 in Fig. 1) and the Beiluo River basin (Sub-Basin 1 in Fig. 1). In order to distinguish the effects of compound dry-hot extreme events over three sub-basins, grid-based datasets were used to make nonstationary risk assessment of compound dry-hot extreme events at regional scale considering climate change.

Monthly precipitation and temperature data (Peng et al., 2019) at 0.0083333° (1 km) spatial resolution ranging from 1901 to 2017 were applied, which were obtained from Loess Plateau Science Data Center, National Earth System Science Data Sharing Infrastructure, National Science & Technology Infrastructure, China (https://loess.geodata.cn). For quantifying significant impacts of compound dry-hot events on humanity and agriculture in summer, the average precipitation (AP) and temperature (AT) during June-July-August (JJA) at each grid were first calculated and then the NCDH under nonstationary conditions was derived using Eqs. (4) and (5).

3. Methodology

A dynamic copula-based framework for the identification of compound dry-hot events and risk assessment considering nonstationarity is presented in Fig. 2. As shown in this figure, the proposed methodology

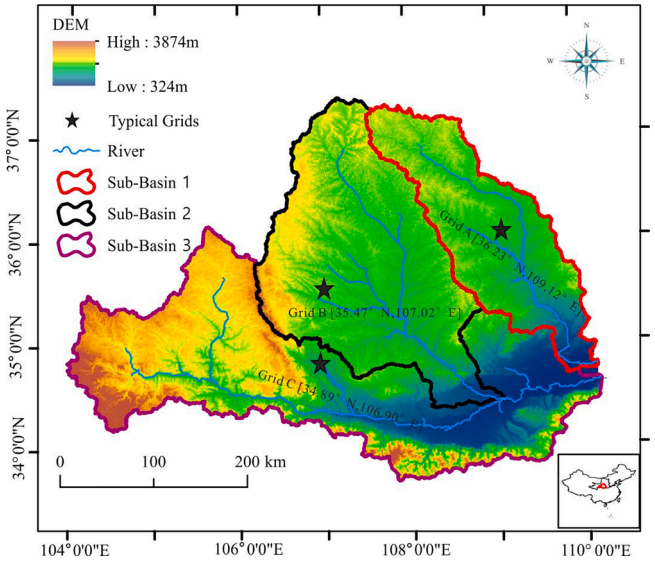

Fig. 1. Study area: Weihe River Basin with three selected grids.

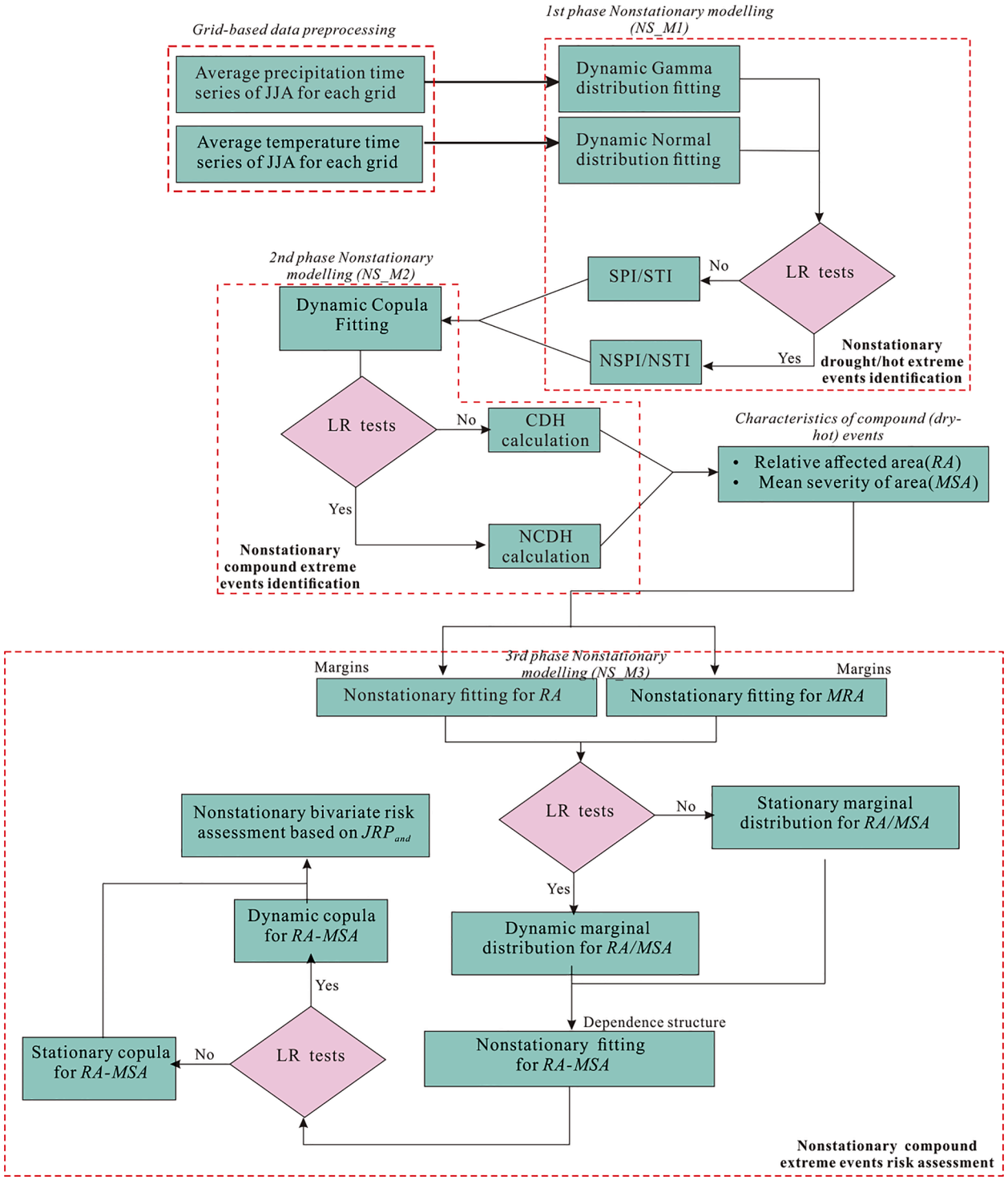

Fig. 2. Flowchart of this study.

involves three phases of nonstationary modelling of the average precipitation (AP) and temperature (AT) time series extracted from grid-based data ($1km \times 1km$): (1) 1st phase (*NS_M1*): applying dynamic gamma distribution for AP and normal distribution for AT through the likelihood ratio (*LR*) test in order to realize the nonstationary identification of drought events by nonstationary standard precipitation index (NSPI) and hot events by nonstationary standard temperature index (NSTI); (2) 2nd phase (*NS_M2*): deriving the compound dry-hot events index (NCDH) from the joint probability of NSPI (or SPI) and NSTI (STI) obtained from dynamic copula fitting; (3) 3nd phase (*NS_M3*): applying nonstationary copula modelling for the dependence structure between two characteristics of dry-hot events (relative affected area (*RA*) and mean severity of area (*MSA*)) which were from extracted grid-based NCDH data under a certain threshold value of NCDH. As shown in the flowchart, the *LR* tests were run through all three phases of modelling in order to assure the rationality of nonstationary detection. A time-varying joint return period under the AND scenario was implemented for nonstationary risk assessment (Salvadori and De Michele, 2004).

It is known that the hydrometeorological system is influenced by large-scale climate patterns, such as El Niño–Southern Oscillation

(ENSO), Southern Oscillation Index (SOI), and North Atlantic Oscillation (NAO) (Wang et al., 2015; Sarhadi and Soulis, 2017). El Niño 3-Southern Oscillation (ENSO), which is derived from the large-scale ocean–atmosphere interactions, had been found been critical driver to the droughts in the Yellow River basin (Dong and Ren, 1996; Wang et al., 2006). Studies showed that precipitation in East Asia could be influenced by the surface temperature (SST) anomalies in the North Pacific Ocean and Indian Ocean, which would lead to the variations of wet/dry conditions in the Yellow River basin (Moy et al., 2002). Wang et al. (2019) applied the cross-wavelet approach to verify the finding that drought in the YRB are highly correlated with ENSO. The Northern Atlantic Oscillation is correlated with the warm phase of the North Atlantic SST, which would be conducive to easterly wind anomalies in northern China and less precipitation or more frequent droughts in the semi-arid subarea in the upper reaches of the Yellow River. Yu et al. (2014) have revealed that fluctuations in NAO in YRB could significantly influence climatic factors, such as air temperature, precipitation. The SOI is the index of ENSO events, like El Niño and La Niña events, and has certain effects on precipitation in YRB (Fu et al., 2007; Li et al., 2016; Meng et al., 2021).

The Niño 3 sea surface temperature (SST) was used as a measure of the amplitude of El Niño 3-Southern Oscillation (ENSO). The Niño 3 SST index (NINO3) was defined as the seasonal SST averaged over the central Pacific (5°S to 5°N, 90°–150°W). In order to reflect the impact of climate change over compound dry-hot events, we employed the three phases of nonstationary modelling, including marginal fitting and copula fitting with distribution parameters incorporating large-scale climate indicators (NAO, SOI and NINO3) as covariates to derive the nonstationary compound dry-hot extreme index (NCDH). Given the NCDH index, nonstationary risk assessment of the compound dry-hot events for each sub-basin at regional scale described by relative affected area (RA) and mean severity of area (MSA) is made.

3.1. Construction of a nonstationary SPI/STI considering climate change

The traditional paradigm of SPI and STI calculations (McKee et al., 1993) involved gamma and normal distributions fitted for different time scales of precipitation and temperature series, respectively, on the basis of stationary hypothesis. Due to substantial anthropogenic activities as well as climate change, the applicability of stationary hypothesis has been challenged (Milly et al., 2008). Instead of considering the time-scale effect of precipitation and temperature data, the nonstationary SPI and STI based on average precipitation (AP) and temperature (AT) during June-July-August (JJA), respectively, was calculated because of the emphasis on dry-hot events during the summer season. For economy of space, we only show the procedure for calculating NSPI, while NSTI was calculated in the same way.

Let s represents the precipitation series. Then, its dynamic probability density function based on the two-parameter gamma distribution can be described as follows:

$$f(x) = \frac{1}{\sigma(t)^{\kappa(t)}} \frac{s^{\kappa(t)-1}\exp\left(-\frac{s}{\kappa(t)}\right)}{\Gamma(\kappa(t))}; \sigma(t)\rangle 0, \kappa(t)\rangle 0 \quad (1)$$

where $\sigma(t)$ and $\kappa(t)$ denote the scale and shape parameters, respectively, and $\Gamma(.)$ is the mathematical function. $\Theta(t) = \{\sigma(t),\kappa(t)\}$, here $\Theta(t)$ is the parameter set composed of $\sigma(t)$ and $\kappa(t)$. Since we incorporated the large-scale climate indicators as covariates of gamma distribution parameters, the assumed linear relation between the large-scale climate indicators and $\Theta(t)$ was established as:

$$\Theta(t) = \begin{cases} constant \\ \Theta_0 + \Theta_1 t \\ \Theta_0 + \Theta_1 Cov(t) \end{cases} \quad (2)$$

where $Cov(t)$ is the time-varying large-scale climate indicator. Time is also assumed as a potential covariate of the parameter sets. In terms of the time-lagging effect on the relation between extreme variables (average precipitation, AP) and large-scale climate indicators (He and Guan, 2014), the NAO/SOI/NINO3 value with 1 month to 3 months prior to the average precipitation series of JJA was considered. Since the focus was on grid-based data, many types of assumed stationary and nonstationary Gamma models (Table S1**(a)**) were checked by the *LR* test for each grid-based AP time series. In considerations of the combined effect of all above covariates (climate drivers and time), we used stepwise model selecting strategy to derive the best-fitted nonstationary models: (1) The corrected Akaike information criterion (AIC_c) combined with LR tests to select the potential models (SGA, NSGA1-NSGA30) in the first step; (2) For the potential models whose AIC_c value of nonstationary model (NSGA1-NSGA30) is less than that of stationary model (SGA), the linear superposition effect of the covariates belonging to the potential nonstationary model in first step by substituting the problem of univariate linear regression (Eq. (2)) into multivariate linear regression problem is considered for secondary optimization analysis through *AICc* criterion and LR tests. Then the best selected nonstationary gamma distribution was transformed into the standard normal distribution to derive the NSPI value for each grid. Let SGAU represent the stationary gamma model for AP, while $NGAU_i$ be a certain time-varying model with trend existing in the parameter. The *LR* test was applied to check whether potential trend-caused nonstationarity would exist or not (Coles, 2001; Xu et al., 2020a, 2020b):

$$LR = 2(LL_{NGAU1_i} - LL_{SGAU}) \quad (3)$$

where LL_{NGAU1_i} represents the maximum likelihood value of every potential nonstationary model (here $NGAU_i$); and LL_{SGAU} is the maximum likelihood value of the stationary model. LL_{SGAU} denotes the null trend assumption. The rejection of the null trend assumption stands for the situation when the p-value of *LR* test was smaller than that at the significance level of 5 %.

The nonstationary models which can pass the *LR* tests should also experience the dynamic goodness of fit (GOF_{k-S}) tests based on the Kolmogorov-Smirnov (*K-S*) test at a significance level of 5 % to verify the fit of the potential nonstationary or stationary gamma models. The corrected Akaike information criterion (AIC_c) was employed to quantify the goodness of fit of the distribution models. The metrics of the best-fitted gamma distribution should correspond to the smallest *AICc* and a relatively smaller or bigger p-value of *LR* ($\leq$ 5%) and *K-S* ($\geq$ 5%) tests.

After the best-fitted dynamic gamma model selection, the cumulative probability of AP series was transformed into NSPI through the standard normal distribution. Parallel to the approach to derive the NSPI index, the NSTI index calculation also involves the nonstationary normal distribution modelling based on the *LR*, and *K-S* tests and *AICc* criterion. The potential nonstationary normal distributions are presented in Table S1**(b).**

3.2. Construction of a nonstationary compound dry-hot index (NCDH) considering climate change

Hao et al. (2019) and Wu et al. (2019, 2020) first proposed the compound dry-hot index (CDH) by establishing the joint probability of bivariate random variables (SPI and STI here) under stationary hypothesis. Parallel to the nonstationary SPI/STI calculation, the nonstationarity should also be incorporated in the process of deriving the CDH index due to the potential link between large-scale climate indicators and extreme events.

Considering nonstationarity, let X and Y represent the drought events quantified by NSPI and the hot events quantified by NSTI, respectively. Since the evaluation of compound dry-hot events focuses on the situation that NSPI is lower than or equal to a particular threshold ($X \leq x$), while NSTI is bigger than or equal to a particular threshold ($Y \geq y$), another variable $Z = -Y$ is defined here to simplify the calculation process. The joint probability distribution of $F_{X,Z}(x,z)$ with time-varying

Table 1
Results of nonstationary modeling for three selected grids of Weihe River basin.

Grid	Attribute	Model	Parameters of model				AIC_c	LR	GOF_{ec}
A	AP^a	NSGA3	σ_1 =0.735 [0.625,0.815]	σ_2 = 0.010 [0.002,0.016]	κ_1 = 3.758 [3.268,4.128]	κ_2 =-0.010 [-0.019,-0.004]	268	3e-3	0.70
	AT^b	NSNM3	μ_1 = 2.947 [2.258,3.657]^c	μ_2 = 1.9e − 4 [8e − 5, 2.8e − 4]	σ_1 = −0.779 [-0.856,-0.707]	σ_2 =3.1e-3 [1.9e-3, 4.2e-3]	217	0.032	0.82
	NSPI-NSTI	NSGAU3	θ_1 =0.267 [0.169,0.358]		θ_2 =-0.237 [-0.305,-0.158]		-85.5	0.013	0.57
B	*AP*	NSGA3	σ_1 =0.212 [0.109,0.305]	σ_2 = 0.013 [0.004,0.18]	κ_1 = 4.358 [3.589,5.059]	κ_2 =-0.014 [-0.023,-0.008]	247	6e-3	0.40
	AT	NSNM11	μ_1 =2.766 [2.548,2.917]	μ_2 = −7.2e − 3 -[9.4e − 3, 6.1e − 3]	σ =-0.608 [-0.725, -0.514]		209	2.3e-4	0.57
	NSPI-NSTI	NSGAU3	θ_1 =0.237 [0.135,0.315]		θ_2 =-0.263 [-0.312,-0.169]		-70.8	0.017	0.68
C	*AP*	NSGA23	σ_1 =-1.239 [-1.671, -0.985]		κ_1 = 5.565 [5.263,6.034]	κ_2 =-0.0512 [-0.0432, -0.0298]	323	4e-4	0.96
	AT	SNM	μ_1 =2.667 [2.698,3.059]		σ =-0.542 [-0.709, -0.446]		214	2.1e-3	0.37
	NSPI-NSTI	NSGAU3	θ_1 =0.195 [0.105,0.287]		θ_2 =-0.267 [-0.357,-0.189]		-62.6	2.3e-5	0.66

Note: [a]AP: average precipitation; [b]AT: average temperature; [c][2.258,3.657] represents the upper and lower boundary of the 95% confidence bands.

parameters can be defined as follows:

$$F_{X,Y}(x,z) = \mathrm{P}(X \le x, Z \le z) = C\left(u, v; \theta_C^t\right) \tag{4}$$

where θ_C^t is the dynamic copula parameters of joint distribution fitted for dependence structure between NSPI and NSTI time series. *uandv* are the marginal distributions of *X* and *Z*, respectively. Parallel to the way of calculating the dynamic gamma parameters as shown in Eq. (2), the large-scale climate indicators are also assumed as potential covariates of copula parameters. The corrected Akaike information criterion (AIC_c) and LR test were employed to quantify the goodness of fit of the distributions. The maximum likelihood method was used to estimate the dynamic copula parameters. The Gaussian copula was found suitable to model both positive and negative dependences among multiple variables (Hao et al., 2017; Van de Vyver and Van den Bergh, 2018), so 11 kinds of nonstationary Gaussian copula (**Table S2**) were selected as the potential copula models to illustrate the joint distribution function.

The dynamic joint probability distribution $F_{X,Z}(x,z)$ can be employed as a metrics to quantify the joint status of dry and hot extreme events under nonstationary conditions. The joint probability distribution $F_{X,Z}(x,z)$ was then transformed to a uniform distribution by using the empirical Gringorten (*EG*) plotting position formula, which was then standardized as a normal index to quantify the severity of compound dry and hot events. Thus, the nonstationary compound drought-hot extreme index (NCDH), based on the standardization of the above *EG* can be expressed as:

$$NCDH = \Phi^{-1}\left\{EG[F_{X,Z}(x,z)]\right\} \tag{5}$$

where the lower NCDH value shows the condition with lower precipitation and higher temperature with negative effects, which is of practical interest. Since nonstationarity has been incorporated into the CDH index, the variations of large-scale climate indicators would lead to the evolution of compound dry-hot extreme event status.

3.3. Definition of compound dry-hot events and their characteristics

After NCDH is derived, thresholds must be set to distinguish individual compound dry-hot events. Similar to the thresholds of SPI to characterize different categories of drought, compound dry and hot conditions can also be classified into several groups according to thresholds. Details of the upper and lower boundary set for the conditions can be found in Wu et al. (2019, 2020). In this study, we set the threshold value as −0.5 to focus on the abnormal compound dry-hot condition ($NCDH < -0.5$). Two kinds of regional characteristics, called relative affected area (*RA*) and mean severity of area (*MSA*), were used to quantify the risk of compound dry-hot extreme events corresponding to each sub-basin. Theoretically, the minimum value of affected area is zero and the maximum affected area is the total area of each sub-basin. For convenience of risk assessment in the following section, we defined the relative affected area (*RA*) and the mean severity of area (*MSA*) as follows:

$$M_t = \frac{N_{grid}^t}{N_{total}} \tag{6}$$

$$RA_t = -ln\frac{1 - M_t}{1 - M_{min}} \tag{7}$$

$$MSA_t = \frac{\sum_{i=1}^{N_{grid}^t} |NCDH_i|}{N_{grid}^t} \tag{8}$$

where N_{grid}^t is the number of grids which corresponds to the abnormal compound dry-hot condition with *NCDH* smaller than −0.5 in year t, while N_{total} is the total number of grids of each sub-basin. M_t is the relative area of the *t*-th year. If we have 60 years of data, M_{min} is the minimum value of $\{M_t, t = 1,2,\cdots,60\}$. In order to make the range of M_t fall in $(0, +\infty)$, Eq. (6) is transformed into Eq. (7) to get RA_t.

3.4. Joint probability distribution for RA and MSA

Here dynamic copula models were used second time to construct the joint distribution of RA and MSA:

$$H(RA, MSA) = \mathrm{P}(RA \le RA_0, MSA \le MSA_0) = C\left(u, v; \theta_C^t\right) \tag{9}$$

where *u* and *v* are the marginal distributions of *RA* and *MSA*. Here RA0 and MSA0 is a random quantile pair of regional characteristics. Before constructing the joint distribution, the nonstationary marginal distribution of *RA* and *MSA* should be determined first. Gamma, normal, log-normal and GEV (Generalized Extreme Value) distributions were assumed as potential margins with dynamic distribution parameters (Eq.

(2)). With the same procedure as for diagnosing the nonstationarity for gamma distribution in section 2.1, 90 kinds of nonstationary functions (Table S1**(a)-(d)**) were considered to ascertain the nonstationarity of *RA* and *MSA* with large-scale climate indices. As shown in section 2.3, 11 kinds of nonstationary Gaussian copula (**Table S2**) were selected as potential copula models to illustrate the joint distribution function.

3.5. Bivariate risk assessment of compound dry-hot events at regional scale

Since compound dry-hot events have two characteristics, the return period from marginal point considering only one characteristic is not enough. On the other hand, due to climate change, the static return period may not be appropriate, which leads to a bivariate time-varying joint return period expressing the risk of compound dry-hot events that was calculated here. In the multivariate frequency analysis, different types of joint return period (JRP), including JRP^{AND}, JRP^{OR}, JRP^{SUR} have been suggested in literature (Salvadori et al., 2013; Shiau, 2006). There is still discussion on which form of the JRP could be more appropriate in water resources planning and project design. We selected the commonly used JRP^{AND} to make a comparison of risk assessment between the stationary and nonstationary cases. The joint return period of *RA* and *MSA* under nonstationary conditions can be defined as:

$$JRP_t^{AND} = \frac{\omega}{1 - F_{RA}^t - F_{MSA}^t + C\left(F_{RA}^t, F_{MSA}^t; \theta_C^t\right)} \tag{10}$$

where F_{RA}^t *and* F_{MSA}^t are the time-varying marginal distributions of *RA* and *MSA*, respectively; $C\left(F_{RA}^t, F_{MSA}^t; \theta_C^t\right)$ is the dynamic copula distribution with time-varying copula parameter; ω is the rate of the number of years in the study period to the number of compound dry-hot events.

4. Results

4.1. Optimal selection of nonstationary models for NSPI, NSTI and NCDH calculation

Here we show results of the first phase and the second phase of nonstationary modelling in order to derive the NCDH index to quantify the severity of compound dry-hot events.

For each grid-based data, a nonstationary gamma and normal model combined with *LR*, *GOF* test and *AICc* optimizing criteria (Eqs. (1)–(3)) was established for average precipitation and temperature records during summer time (JJA), respectively. Since there were 190,975 grids in this study, three typical grids (Grids A, B and C in Fig. 1) were chosen to show the detailed information of the nonstationary models. In order to evaluate the model uncertainty, the parametric bootstrap method was used to analyze the uncertainty of the fitted models (Serinaldi and Kilsby 2015).

Considering the potential link between large-scale climate indices and *AP* or *AT*, almost 30 kinds of nonstationary gamma and normal models incorporating different climate indices and time as covariates of distribution parameters were considered (Table S1**(a)-(b)**). For all three grids (A-C), NSGA3 with both parameters showing a linear relation with time (year in this study) proved to be the most suitable model for fitting the average precipitation (AP) observations. Different from nonstationary normal distribution for AT in Grid A with distribution parameters showing a linear relation with time, two parameters of the nonstationary normal model for AT in Grid B and C showed a linear relation with 3-month time-lagging North Atlantic Oscillation (NAO_3 shown in **Table S1**). The slope value of gamma parameters for Grid A ($\sigma_2 = 0.01, \kappa_2 = -0.01$ for AP) was relatively smaller than that of Grid B ($\sigma_2 = 0.013, \kappa_2 = -0.014$ for AP) and C ($\sigma_2 = 0.0318, \kappa_2 = -0.0512$ for AP), which showed that the degree of trend-caused nonstationarity in AP of Grid B and C was stronger than that in AP of Grid A. Once the first phase of nonstationary modeling of AP and AT was done, the NSPI and NSTI indices were derived by transforming the cumulative probability of AP and AT series under nonstationary conditions into the standard normal distribution.

In the second phase of nonstationary modelling, a dynamic copula was fitted for the dependence structure of NSPI and NSTI (Table 1). The nonstationary Gaussian copula with 2-month time-lagging North Atlantic Oscillation (NAO_2) as covariates of copula parameter was the best model fitted for the dependence structure between NSPI and NSTI in Grids A and B. NAO_3 was the significant climate index for Grid C. In order to show the quality of model fitting, visual analysis based on worm plot and diagonal plot for copula for marginal distribution and copula are shown in Fig. 3, respectively, which helped verify the rationality of nonstationary models with large-scale climate indices as covariates. As shown in Fig. 3, the selected nonstationary marginal models and Gaussian copula for Grid A, B, and C showed a reasonable model fitting efficiency.

Fig. 4 summarizes the optimal nonstationary models incorporating different climate indices as significant covariates of distribution parameters for AP and AT observed at all 190,975 grids of Weihe River basin. For AT modelling, 2.15 % of grids in Sub-Basin 1 did not show significant nonstationarity, while 64.27 % in Sub-Basin 2 and 30.39 % in Sub-Basin 3 did not show significant nonstationarity. Time plays a leading role in reproducing the undulating behavior exhibited by the average temperature observations in Sub-Basin 1 (Model NSNM2 occupied 48.36 % and NSNM3 occupied 49.48 %). Except for 64.27 % of grids fitted by stationary normal models in Sub-Basin 2, nonstationary models incorporating time and NAO_3 as significant covariates occupied 20.9 % and 14.75, respectively. For grids in Sub-Basin 3,NAO_3 was the main significant covariate for the location parameter of the normal distribution fitted to AT. Different from the model patterns for AT with only NAO_3 and time as significant covariates, NAO_2, $NINO_1$, and $NINO_3$ became the significant covariates in gamma parameters fitted to AP in the whole river basin. For nonstationary modelling of the dependence structure of NSPI and NSTI, NAO_3 played a leading role in causing time-varying variations of relation between drought and hot events. As shown in Fig. 4**(a)-(c)**, the significant covariates for each grid were different from each other due to the spatial variation in precipitation and temperature over the river basin. Owing to the spatial heterogeneity of the nonstationary models fitted for AT, AP and their dependence structure, most of study area showed the necessity of using nonstationary index (NCDH) to quantify the severity of compound dry-hot events (only 6.9 % of Sub-Basin 2 and 8.49 % of Sub-Basin 3 showed CDH).

4.2. Comparison of two indices: CDH and NCDH

To better illustrate the differences among the two indices, we present the time series of compound dry-hot event index for three selected grids in Fig. 1 (Grid A [36.23°N, 109.12°E] in Sub-Basin 1, Grid B [35.39°N, 107.02°E] in Sub-Basin 2, and Grid C [34.89°N, 106.90°E] in Sub-Basin 3) from 1901 to 2017 (see Figs. 1 and 5). Totally speaking, the similar pattern of temporal variations shown by Fig. 5 demonstrates the consistency of CDH and NCDH indexes in exhibiting the dry-hot event propagation process. However, the severity of compound dry-hot events quantified by the two indices distinguished from each other in several years (1939, 1945, 1997, 2006), especially in peak regions of series. For instance, the compound dry-hot condition in 2006 was assigned to be the extreme level by CDH ($= -1.67$), while the severe level by NCDH ($= -1.33$) for Grid A belonging to Sub-Basin 1. For Grid C belonging to Sub-Basin 3, the compound dry-hot condition in 2006 was assigned to be the severe level by CDH ($= -1.38$), while the extreme level by NCDH ($= -1.64$). According Cheng et al. (2014) and Ji & Duan (2020), the extreme level of compound dry-hot condition happened during May to August in Sub-Basin 3, while severe level of compound dry-hot condition happened during summer time in Sub-Basin 1. The difference in severity of compound dry-hot events happened in these two Sub-Basins are attributed to the return of farmland to forest implemented in Sub-Basin 1

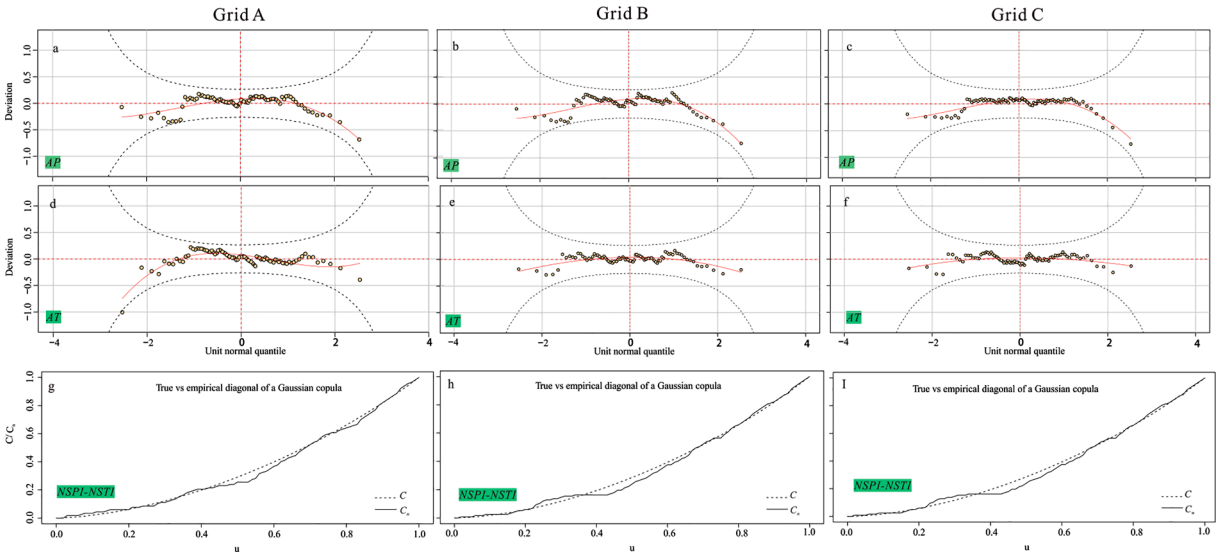

Fig. 3. Worm plot for marginal distrbution and diagonal plot for Copula. For a satisfactory fit, the data points should be within the two black dotted lines (95% confidence interval) in the worm plot, and the theoretical model should be close to empirical copula in the diagonal plot.

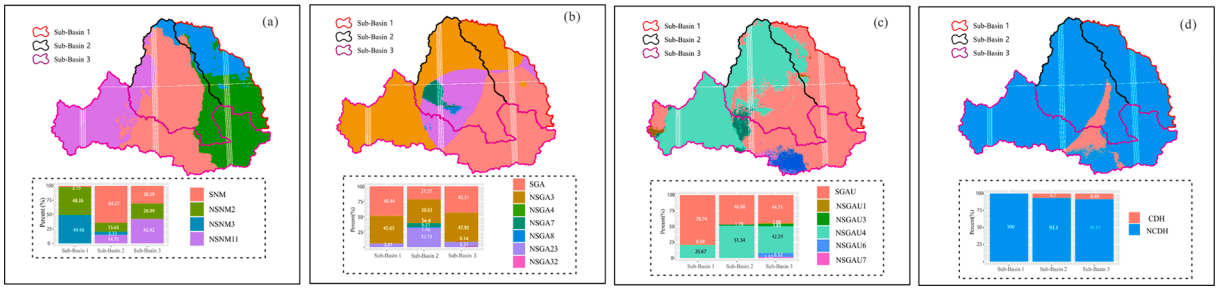

Fig. 4. Summary of the Optimal Nonstationary Models fitted for AP, AT and NSPI-NSTI and final NCDH calculation according to 190,975 grids of data in Weihe River basin. (a) Optimal models for AT. SNM: stationary normal model, NSNM2: nonstationary normal model with time as covariates of location parameter, NSNM3: nonstationary normal model with time as covariates of location and scale parameter, NSNM11: nonstationary normal model with NAO_3 as covariates of location parameter; (b) Optimal models for AP. SGA: stationary gamma model, NSGA3: nonstationary gamma model with time as covariates of shape and scale parameter, NSGA4: nonstationary gamma model with NAO_1 as covariates of scale parameter, NSGA7: nonstationary gamma model with NAO_2 as covariates of scale parameter, NSGA8: nonstationary gamma model with NAO_2 as covariates of shape parameter, NSGA23: nonstationary gamma model with $NINO_1$ as covariates of shape parameter, NSGA30: nonstationary gamma model with $NINO_3$ as covariates of shape and scale parameter; (c) Optimal copula for NSPI-NSTI. SGAU: stationary Gaussian copula, NSGAU1: nonstationary Gaussian with time as covariates of parameter, NSGAU3: nonstationary Gaussian with NAO_2 as covariates of parameter, NSGAU4: nonstationary Gaussian with NAO_3 as covariates of parameter, NSGAU6: nonstationary Gaussian with SOI_2 as covariates of parameter, NSGAU7: nonstationary Gaussian with SOI_3 as covariates of parameter; (d) Spatial distribution of CDH and NCDH.

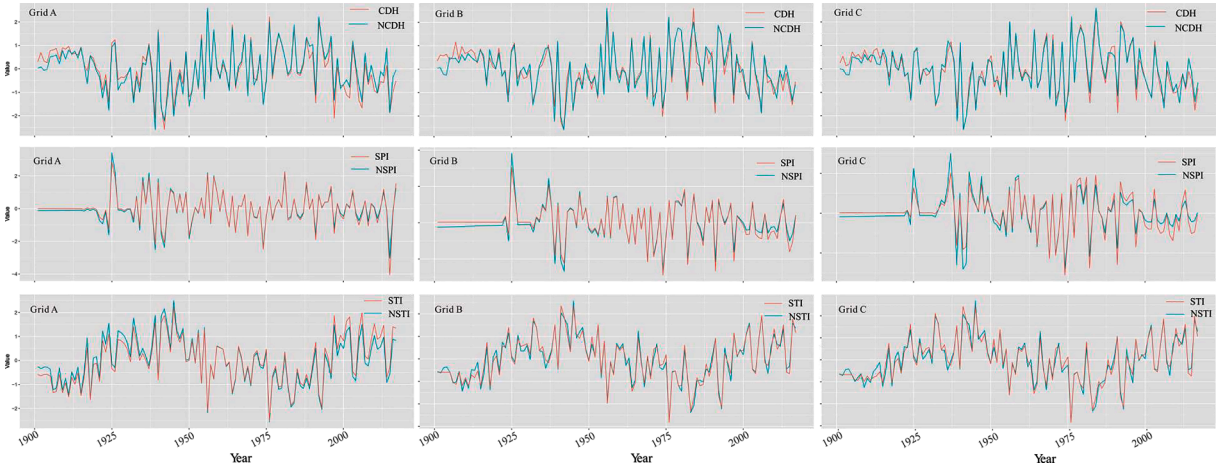

Fig. 5. The time series of CDH, NCDH, SPI, NSPI, STI and NSTI at three selected grids from 1901 to 2017. The location information of the three grids can be seen in Fig. 1.

(Ji & Duan, 2020).

Since the CDH and NCDH were derived from SPI/NSPI and STI/NSTI, the difference of probability density function (PDF) fitted for AP and AT under stationary and nonstationary conditions would pose a great impact on disparities between CDH and NCDH (Fig. 6). Evident differences can be observed in the PDF of precipitation or temperature series, for example, in 1924, 1944 at Grid A; in 1924, 2004 at Grid B; and in 1924, 1944, 1984 and 2004 at Grid C, which is in accordance with differences of the compound dry-hot indices series shown in Fig. 5. The PDF curve of selected grids clearly indicated the difference between NSPI and SPI or NSTI and STI, which led to the difference between CDH and NCDH.

We further compared the differences between the two indices of CDH and NCDH from a spatial perspective in Fig. 7. Fig. 7**(a)** shows a similar spatial pattern exhibited by these two indices with a high correlation value in 1934, 1943, 1957, 1969, 1982, 1994, and 2016 in Fig. 7**(b)**. Focusing on year 2016, the condition of compound dry-hot events in Sub-Basin 1 was in the abnormal level by NCDH, while the condition was in the extreme level by CDH. Focusing on Sub-Basin 3 in 2016 quantified by CDH, the affected area in the upper reaches of Sub-Basin 3 was significantly higher than that in the lower reaches, while NCDH showed the opposite situation. From historical records (Ji & Duan, 2020), more area suffered from dry-hot events in the downstream of Sub-Basin 3 in 2016 than that of upper stream due to higher economic growth and the intensification of urbanization in the downstream over the past few years. Overall, the nonstationarity of precipitation or temperature to derive SPI and STI cannot be ignored in compound dry-hot extreme assessment under climate change, since remarkable difference was observed between stationary index (CDH) and nonstationary indices (NCDH). Furthermore, accurate description of the time distribution of CDH can be derived to help provide more information about the trend of compound dry-hot extremes in time and space.

4.3. Nonstationary copula modelling for RA and MSA

Before copula modelling of the dependence structure between *RA* and *MSA*, pre-experiment of investigating the correlation between them was conducted to check whether *RA* and *MSA* can be analyzed jointly or not. The correlation value between *RA* and *MSA* corresponding to Sub-Basins 1, 2, 3 were 0.821, 0.819 and 0.795, respectively, which showed that the above two characteristics of compound dry-hot events can be further analyzed by copula.

The same optimization process of best-fitted margins and copula as in Section 4.1 was re-operated here for RA and MSA in Table 2. *RA* and

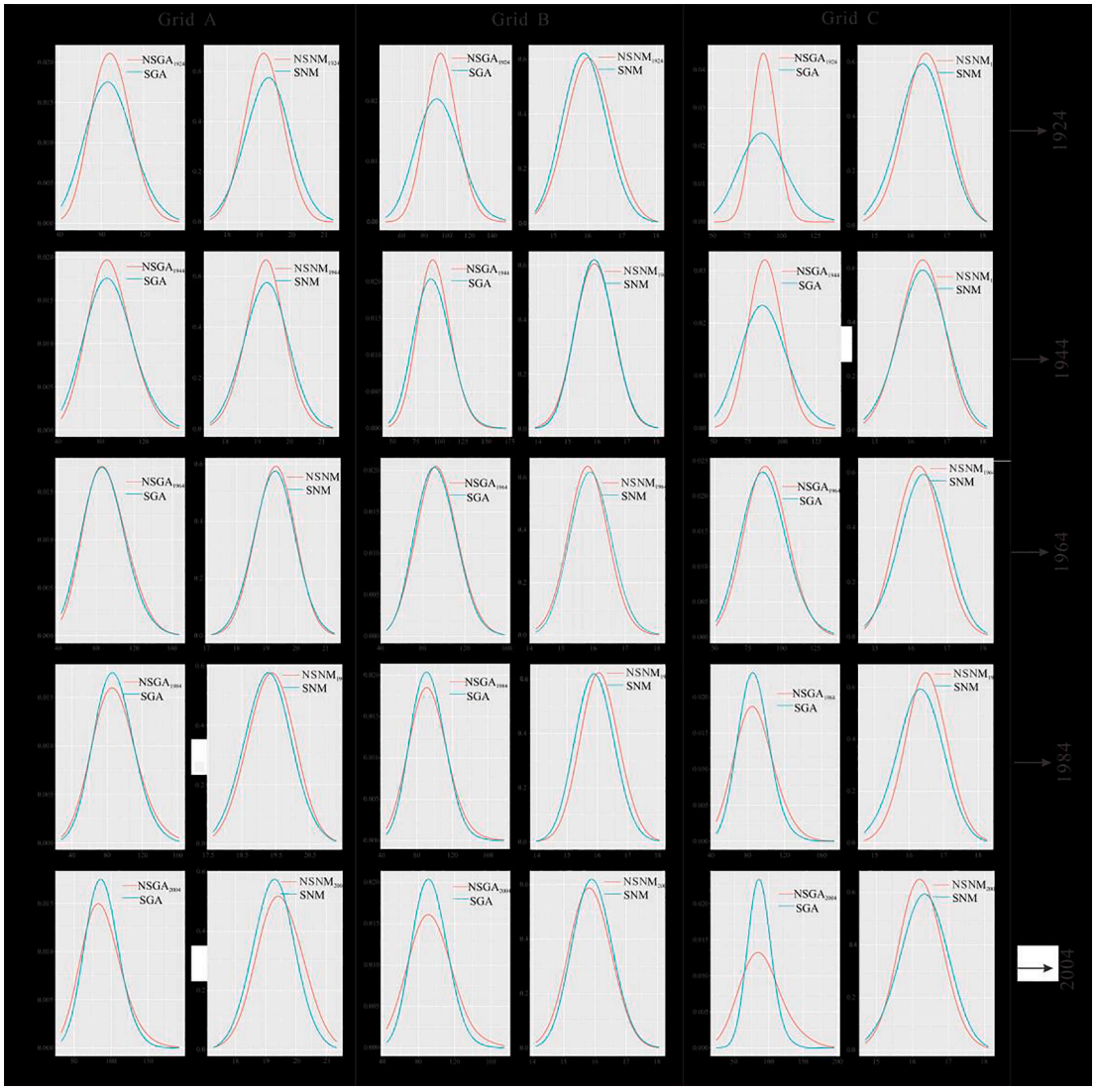

Fig. 6. Comparison of the probability density functions (PDFs) of SPI, NSPI, STI and NSTI at the three selected grids for years 1924, 1944, 1964, 1984, and 2004. $NSGA_{1924}$ denotedsthe nonstationary (time-varying) gamma distribution (in Table 1) at year 1924.

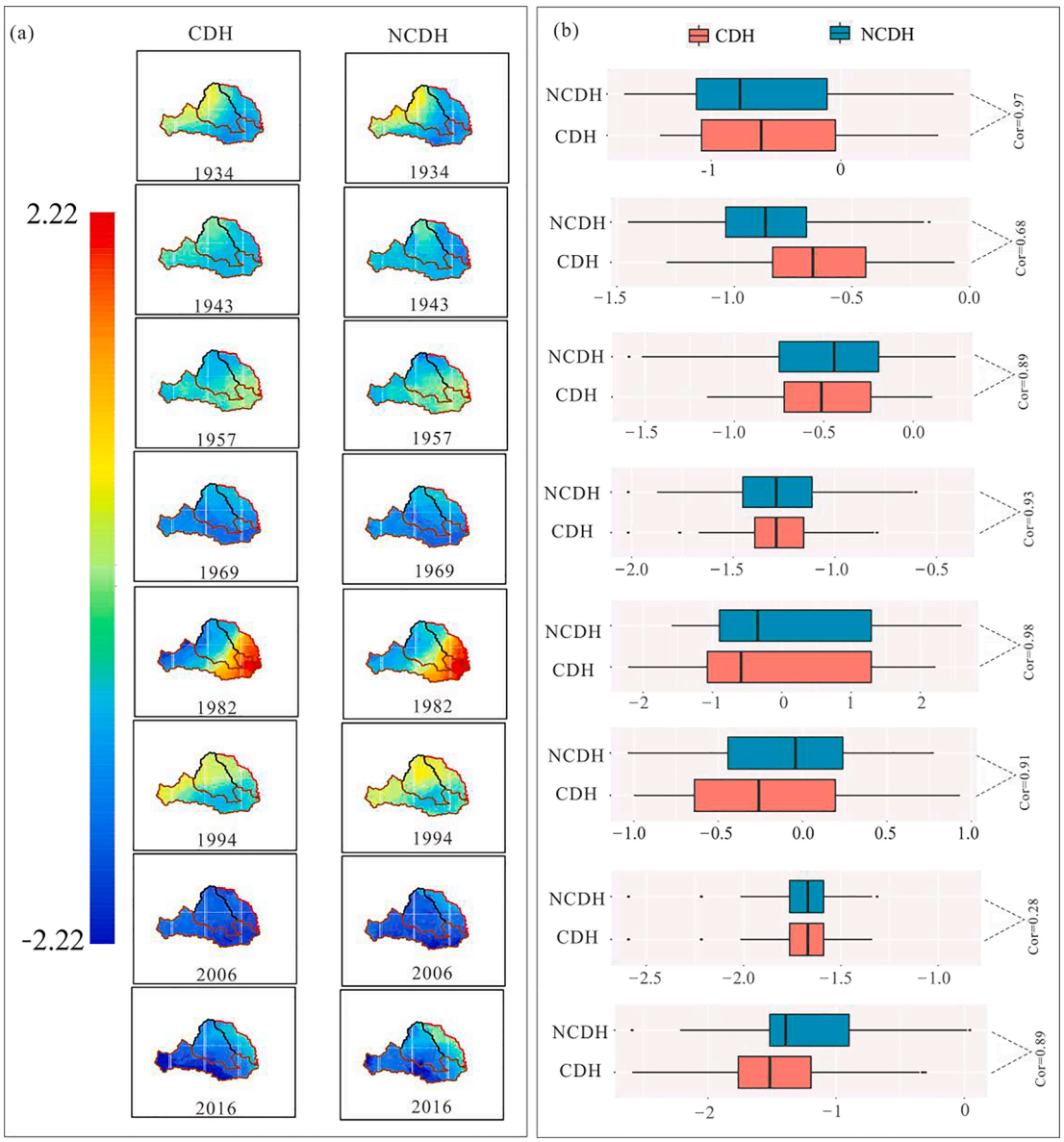

Fig. 7. Comparison of CDH and NCDH in describing the compund dry-hot events in spatial distributions. (a) Regional illustration of CDH and NCDH in Weihe River basin; (b) Boxplot of the spatial distribution of CDH and NCDH for each year.

MSA extracted from Sub-Basin 1 showed no nonstationarity in the process of marginal distribution or copula modelling. When it came to Sub-Basin 2, the dependence structure between *RA* and *MSA* exhibited nonstationarity with the Gaussian copula parameter incorporating NAO_2 as covariates. For Sub-Basin 3, only the marginal distribution for *RA* satisfied the nonstationary situation with SOI_2 as a covariate. Although almost all grids of the study area showed nonstationarity in the process of deriving NCDH (Section 4.1), the regional features of abnormal compound dry-hot events showed a lower degree of nonstationary characteristics (two of nine margins and dependence structure showed nonstationarity).

4.4. Nonstationary risk assessment of RA and MSA

With the joint distribution selected in view of nonstationarity for each sub-basin, the nonstationary risk assessment was analyzed. The design values of indexes characterizing the compound dry-hot events that happened in each sub-basin were computed, based on the And joint return period (JRP). Figs. 8(a,b) present the JRP-isolines of the two characteristics at return levels equaling 50, 20 and 10 years for the three sub-basins. A parametric bootstrap method combined with 90 % ellipse confidence interval (Gu et al., 2020) was adopted in this study to quantify the uncertainty of design values. Since stationary margins and stationary copula were the best-fitted models for Sub-Basin 1 (Table 2), stationary JRP-isolines of the two characteristics belonging to Sub-Basin 1 are plotted in Fig. 8(a). Focusing on ellipse confidence bands at different JRP-isolines, bigger ellipse confidence bands fell on high-level JRP-isolines, which means that uncertainty was negatively proportional to risk of occurrence of compound dry-hot event. The JRP-isolines of Sub-Basin 2 showed little or no obvious changes, especially in the range scale of marginal design values among four selected years, which were caused by the stationary features of marginal distributions and only copula was found to have nonstationarity. When it came to JRP-isolines of Sub-Basin 3, the design values of *RA* varied over time due to the nonstationary gamma distribution with climate indicator, SOI_2 as a covariate for *RA*. From the horizontal perspective of plots, i.e., the variation of *RA* values, the JRP-isolines moved leftward first from 1929 to 1950 and then rightward from 1950 to 2002. Due to the limited

Table 2
Results of nonstationary modeling of *RA* and *MSA* for three Sub-Basins of Weihe River. MSA: mean severity of area; RA: Relative affected area by compound extremes.

sub-basin	Attribute	Model	Parameters of model			AIC_c	LR	GOF_{ec}
1	*RA*	SGA	σ =5.960 [5.734,6.217]	κ =0.491 [0.316,0.663]		112	—	0.86
	MSA	SGEV	μ =0.710 [0.645,0.796]	σ =0.200 [0.144,0.306]	κ =0.506 [0.195,0.936]	125	—	0.98
	RA-MSA	SGAU	θ=0.878 [0.805,0.945]			-36.9	—	0.87
2	*RA*	SGA	σ =6.232 [6.023,6.398]	κ =0.421 [0.238,0.589]		108	—	0.76
	MSA	SGEV	μ =0.716 [0.645,0.800]	σ =0.212 [0.157,0.317]	κ =0.394 [0.126,0.874]	128	—	0.56
	RA-MSA	NSGAU3	θ_1 =1.137 [0.748,1.248]	θ_2 =0.143 [0.078,0.199]		-24.9	0.021	0.68
3	*RA*	NSGA17	σ =4.362 [4.089,4.598]	κ_1 =-0.836 [-1.158,-0.518]	κ_2 =-0.243 [-0.319,-0.159]	108	0.013	0.71
	MSA	SGEV	μ =0.701 [0.616,0.788]	σ =0.192 [0.156,0.247]	κ =0.445 [0.168,0.756]	134	—	0.68
	RA-MSA	SGAU	θ=0.869 [0.798,0.937]			-25.8	—	0.79

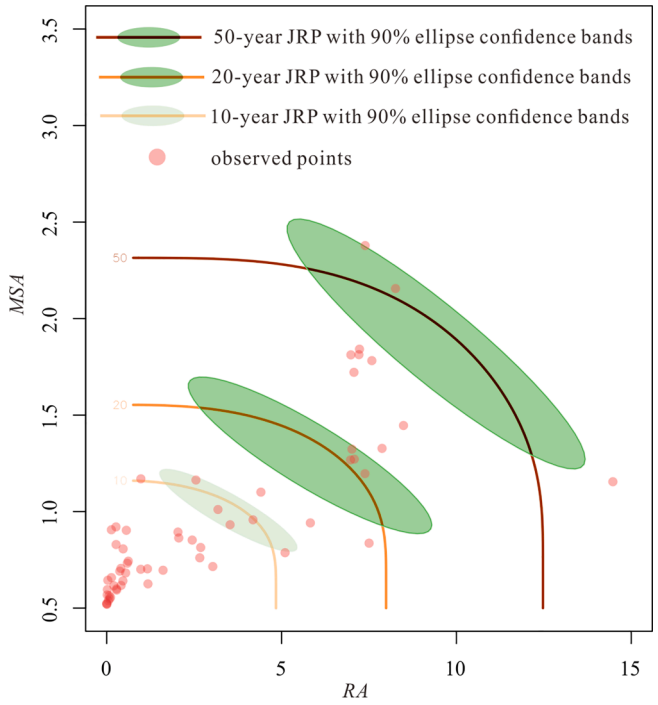

Fig. 8a. Joint return period (JRP) of Sub-Basin 1 based on stationary magins and copula fitted for *RA* and *MSA*. Uncertainty of JRP was quantified by the parametric bootstrap method to derived the 90% ellipse confidence bands.

number of plots, we just present here the overall variation of the design value of RA changing with time-varying SOI_2, and the exact pattern of the variation of joint distribution can be addressed from the complete set of plots. Comparing JRP-isolines between Sub-Basins 2 and 3, the nonstationarity in the marginal distribution (nonstationary gamma model for RA of Sub-Basin 3) could cause more time-varying variations of design values at each return level than that in the dependence structure (nonstationary Gaussian copula for *RA-MSA* of Sub-Basin 2) between *RA* and *MSA*.

4.5. *Discussion of different kinds of nonstationary scenarios over risk assessment results*

Since the nonstationary risk assessment of compound dry-hot events was applied, based on three phases of nonstationary modelling: (1) 1st phase (*NS_M1*): nonstationary gamma distribution for AP and normal distribution for AT to calculate NSPI and NSTI, respectively; (2) 2nd phase (*NS_M2*): using dynamic copula 1st time for fitting the dependence structure between NSPI and NSTI to derive NCDH using Eqs. (4) and (5); and (3) 3nd phase (*NS_M3*): using the dynamic copula 2nd time for the dependence structure between *RA* and *MSA*.

It is of great interest to investigate how the final risk assessment results would be influenced by considering nonstationarity or not during the 1st and 2nd modelling phases. As a result, five kinds of scenarios were considered to answer the above issue: (1) scenario 0: the stationary modelling was implemented in all three phases (*S_M1-S_M2-S_M3*); (2) scenario 1: nonstationary modelling was implemented in all three phases (*NS_M1-NS_M2-NS_M3*) which has been realized in Section 4.4; (3) scenario 2: stationary modelling was implemented in the 1st and 2nd phases while nonstationary modelling was implemented in the 3rd phase (*S_M1-S_M2-NS_M3*); (4) scenario 3: stationary modelling was implemented in the 1st phase, while nonstationary modelling was implemented in the 2nd and 3rd phases (*S_M1-NS_M2-NS_M3*); and (5) scenario 4: nonstationary modelling was implemented in the 1st phase, while stationary modelling was implemented in the 2nd and 3rd phases (*NS_M1-S_M2-NS_M3*). We used scenario 0 as a benchmark to show the time-varying JRP-isolines. Detailed information of modelling results in the 3rd phase of nonstationary modelling of *RA* and *MSA* under scenarios 2–4 is shown in Table S3(a)-(c) and results of the JRP-isolines corresponding to Scenarios 0, 2, 3, and 4 are exhibited in Fig. S1**(a)-(e)**. Based on the results of Table S1**(a)**, the occurrence risk of compound dry-hot events in Sub-Basin 1 was significantly lower than that in the other two basins, which was because the design values of MSA and RA in Sub-Basin 1 at the same joint return level were smaller than those of the

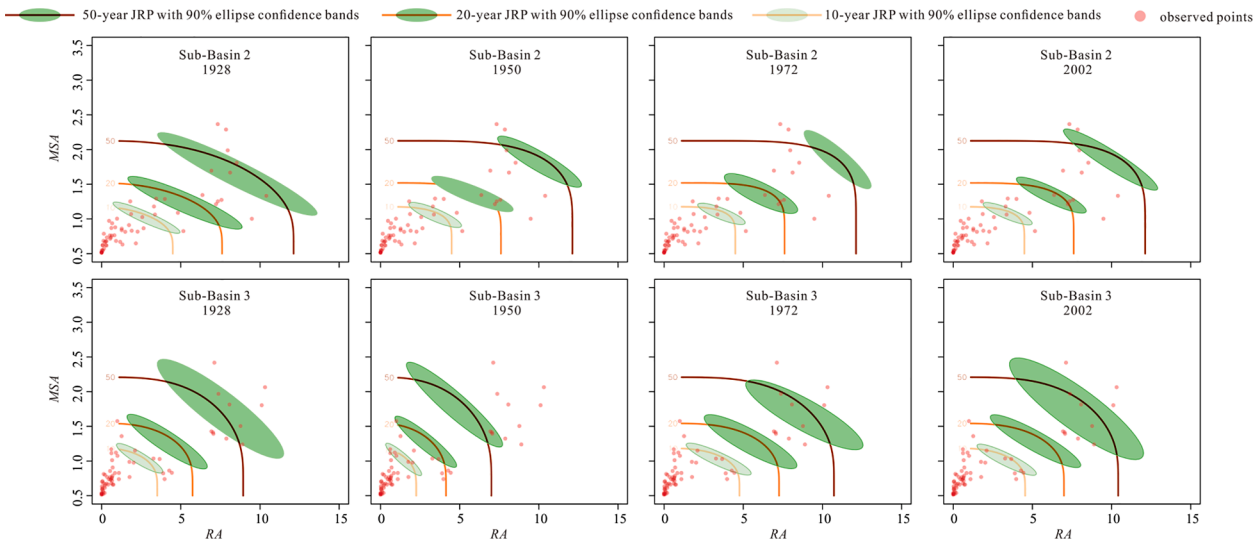

Fig. 8b. Joint return period (JRP) of Sub-Basins 2 and 3 based on nonstationary magins or nonstationary copula fitted for *RA* and *MSA*. Uncertainty of JRP was quantified by parametric bootstrap method to derived the 90% ellipse confidence bands.

other two basins.

Comparison of nonstationary modelling results and results of the JRP-isolines between Scenarios 1 and 4 would help identify the effect of considering nonstationarity in the 2nd modelling phase over results of risk assessment. Focusing on the nine cases of modelling results in Table 2 and **Table S3(c)**, the similar results of the 3rd nonstationary modelling existed between Scenarios 1 and 4: the dependence structure of MSA and RA in Sub-Basin 2 and marginal distribution of RA in Sub-Basin 3 both showed nonstationarity with the same climate indices as covariates (NAO_2 for copula parameter of Sub-Basin 2 and SOI_2 for the scale parameter of Sub-Basin 3). Other seven cases of three sub-basins under Scenarios 1 and 4 showed no nonstationarity. Comparison of JRP-isolines under these two scenarios (Figs. 8(a)-(b) and Fig. S1(d)-(e)) also showed the similar pattern of time-varying variations of design values at return levels of 10, 20, and 50 years.

In the same way, comparisons of JRP-isolines and results of 3rd modelling results under scenarios 1 and 3 would investigate the effect of considering nonstationarity in the 1st modelling phase over results of risk assessment. As shown in the nine cases of modelling results in Table 2 and **Table S3(b), 5** cases of modelling results showed nonstationarity under scenario 3, which was significantly distinguished from those (only t20 cases) under scenario 1. The same conclusion can be drawn through visual comparison of JRP-isolines between Fig. 8 and Fig. S1**(c)**. As shown in Table 2 and **Table S3(b)**, considering nonstationarity caused by climate indices in average precipitation and temperature series during the 1st modelling phase would help reduce the complexity of subsequent risk analysis based on characteristic variables of compound extreme events, which was because of less cases showing nonstationarity in the 3rd modelling phase under scenario 1.

In summary, whether considering nonstationarity in the 2nd phase modelling or not would pose little impact on the nonstationary risk assessment results of compound dry-hot event, while nonstationarity in the 1st phase modelling of average precipitation and temperature could make a difference over nonstationary risk assessment of compound dry-hot events. In other words, nonstationarity in average precipitation and temperature should be consequently recognized as the more dominant factor in nonstationary risk analysis of compound dry-hot events than the nonstationarity in the dependence structure between SPI and STI.

5. Discussion

This study proposed the dynamic Copula model to link the SPI and STI index to identify and make the risk evaluation of compound dry-hot events from the perspective of nonstationarity. As the drought or dryness monitoring and assessing index, the Standardized Precipitation Index (SPI) are derived from precipitation only, which showed a potentially significant limitation of omission of evapotranspiration (Vicente-Serrano et al., 2010; Potop et al., 2012; Chen et al., 2016; Um et al., 2017). The Standardized Precipitation Evapotranspiration Index (SPEI), proposed by Vicente-Serrano et al. (2010), could offer better performance of drought impact evaluation (Begueria et al., 2014; Gao et al., 2017; Parsons et al., 2019; Pei et al., 2019). Instead of focusing on average precipitation (AP) during JJA (June-July-August) for SPI in this study, the time series of average water balance (AWB) of JJA, which is difference between precipitation and potential evaporation (ET_0), needs to be investigated by the LR tests to verify the potential nonstationarity. The nonstationarity of AWB time series would also be a key factor to influence the nonstationary compound dry-hot index (NCDH). As the emphasis of this work was on the impact of the identification and risk assessment of compound dry-hot events imposed by the potential nonstationarity existed in the precipitation and temperature series, the nonstationary SPEI index considering precipitation and evaporation comprehensively would be addressed in our future study of compound dry-hot events.

In order to explore the rationality of the nonstationary compound dry-hot index adopted in this study, the proposed compound index was also addressed in another catchment: Fenhe River Basin (FRB) **(Fig. S2)** to check whether one would expect the index to be consistent in space for nearby catchments. As shown in Fig. S3**(a)-(c)**, nonstationary Gamma models (NSGA32) occupied 71.8 % of grids for AP series while nonstationary normal models (NSNM5 (47.3 %) and NSNM34(52.7 %)) was the best-fitted models at all grids for AT series in FRB. Although only 4.1 % of grids for dependence structure between NSPI and NSTI recommended nonstationary Gaussian Copula (NSGAU15) models, the nonstationary compound dry-hot index should be taken into consideration for the whole catchment because of the nonstationarity existed at all grids for AT series. **Fig. S4** helped verify the consensus spatially: the nonstationarity of precipitation or temperature to derive SPI and STI cannot be ignored in compound dry-hot extreme assessment under climate change, since remarkable difference could be identified for the comparison of CDH and NCDH index in FRB.

We could make a short-term prediction of compound dry-hot events as follows: Since the larger-scale climate indexes were the climate indicators of the previous 1–3 months, the nonstationary NCDH-based models can be used to make 1–3 month-lead prediction of the likelihood of the regional compound dry-hot extreme events once we get the

value of climate indicators at present. For a long-term prediction of the compound dry-hot events, a systematic projection of the compound dry-hot events would be feasible with the help of the global climate model (GCM) simulations involved in Coupled Model Inter-comparison Project Phase 6 (CMIP6).

6. Conclusions

In this study, a nonstationary framework for the identification of compound dry-hot extremes and risk assessment is proposed to explore the potential evolution regime over the past 117 years in Weihe River Basin (WRB) and Fenhe River Basin (FRB). It consists of three phases of nonstationary modelling of the average precipitation (AP) and temperature (AT) time series extracted from grid-based data ($1km \times 1km$). The first phase modelling of nonstationary gamma distribution of AP and normal distribution of AT with large-scale climate indices as covariates was implemented to derive the nonstationary SPI (NSPI) and STI (NSTI), respectively. The first-time nonstationary copula modelling of dependence structure between NSTI and NSOI was applied to derive the nonstationary compound dry-hot extreme index (NCDH) in the 2nd phase. Based on nonstationary modelling of the first two phases, comparison of NCDH and CDH to identify historical compound dry-hot events were also made in this study. With the threshold value of NCDH being set as -0.5, two regional characteristics of compound extremes, relative affected area (*RA*), and mean severity of area (*MSA*) could be extracted from the grid-based datasets. The second time nonstationary copula modelling of dependence structure between RA and MSA was investigated to make nonstationary risk assessment of compound dry-hot events in the WRB. The main findings of this study can be summarized as follows:

1) From the results of nonstationary modelling in the 1st and 2nd phases, most area of WRB showed the necessity of using nonstationary index (NCDH) to quantify the severity of compound dry-hot events (only 6.9 % of Sub-Basin 2 and 8.49 % of Sub-Basin 3 showed CDH) due to the spatial heterogeneity of nonstationary models fitted for AT, AP and their dependence structure.
2) Compared with stationary CDH (Hao et al., 2019; Wu et al., 2019, 2020), the main properties of NCDH can be concluded as follows: (a) NCDH combines large-scale climate indices with lead times of 1–3 months (NAO, SOI, NINO3), thus incorporating climate change in calculating NCDH; (b) The performance of reconstructing historical compound extremes by NCDH was better than that by CDH; (c) Due to the dynamic response to the evolution of the probability distribution function (PDF) over time, the proposed NCDH provided more robustness and rationality for drought assessment under climate change.
3) Based on JRP-isolines of *RA* and *MSA* in the three sub-basins, the nonstationarity in the marginal distributions had a more impact on the design values at each return level than that in the dependence structure. The uncertainty was negatively proportional to risk of occurrence of compound dry-hot event.
4) Based on different kinds of nonstationary scenarios over nonstationary risk assessment, nonstationarity in average precipitation and temperature should be paid more attention in the 1st modelling phase to derive SPI and STI indexes. Compared to nonstationarity in the 1st modelling phase, nonstationarity in the dependence structure between SPI and STI, which was the 2nd modeling phase, had a less impact over risk assessment.

We used the time-varying copula-based model incorporating different large-scale climate indices as covariates mainly to make the dynamic identification and risk assessment of compound dry-hot events in WRB. The proposed framework identified compound dry-hot events with high-efficiency as well as their evolution tracks, and the nonstationary feature of compound dry-hot frequency analysis helps understand the evolution and characteristics of compound dry-hot events more comprehensively. Much expansive work should be carried out to overcome the potential deficiency of this framework. For instance, other physically induced indexes, such as GDP, and land use-related index should also be considered. In this study, SPI and STI were used to derive the nonstationary compound dry-hot monitoring index (NCDH). Other standardized indexes like SPEI considering evapotranspiration effect should also be considered to calculate NCDH in a future study.

CRediT authorship contribution statement

Pengcheng Xu: Methodology, Formal analysis, Writing – original draft, Writing – review & editing. **Dong Wang:** Conceptualization, Writing – review & editing, Supervision. **Yuankun Wang:** Conceptualization, Supervision, Project administration. **Vijay P. Singh:** Conceptualization, Writing – review & editing. **Jianchun Qiu:** Writing – review & editing. **Jichun Wu:** Writing – review & editing, Project administration. **Along Zhang:** Writing – review & editing. **Xiaopei Ju:** Writing – review & editing.

Declaration of Competing Interest

The authors declare that they have no known competing financial interests or personal relationships that could have appeared to influence the work reported in this paper.

Data availability

The data that has been used is confidential.

Acknowledgments

Acknowledgement for the data support from “Loess plateau science - data center, National Earth System Science Data Sharing Infrastructure, National Science & Technology Infrastructure of China (http://loess.geodata.cn).” The grid-based precipitation and temperature datasets can be downloaded from http://loess.geodata.cn/data/datadetails.html?dataguid = 192891852410344&docid = 5 and http://loess.geodata.cn/data/datadetails.html?dataguid = 164304785536614&docid = 213.

This study was supported by the Natural Science Foundation of Jiangsu Province (BK20220589) and the National Key Research and Development Program of China (2020YFC1807801).

Appendix A. Supplementary data

Supplementary data to this article can be found online at https://doi.org/10.1016/j.jhydrol.2022.128852.

References

Abatzoglou, J.T., Rupp, D.E., O’Neill, L.W., Sadegh, M., 2021. Compound extremes drive the western Oregon wildfires of September 2020. Geophys. Res. Lett. 48 e2021GL092520.

Agilan, V., Umamahesh, N.V., 2017. What are the best covariates for developing non-stationary rainfall intensity-duration-frequency relationship? Adv. Water Resour. 101 (MAR.), 11–22.

Alizadeh, M.R., Adamowski, J., Nikoo, M.R., AghaKouchak, A., Dennison, P., Sadegh, M., 2020. A century of observations reveals increasing likelihood of continental-scale compound dry-hot extremes. Sci. Adv. 6, eaaz4571.

Begueria, S., Vicente-Serrano, S.M., Reig, F., Latorre, B., 2014. Standardized precipitation evapotranspiration index (SPEI) revisited: parameter fitting, evapotranspiration models, tools, datasets and drought monitoring. Int. J. Climatol. 34 (10), 3001–3023.

Bender, J., Wahl, T., Jensen, J., 2014. Multivariate design in the presence of non-stationarity. J. Hydrol. 514, 123–130.

Blöschl, G., Hall, J., Parajka, J., Perdigão, R.A.P., Merz, B., Arheimer, B., Živkovic, N., 2017. Changing climate shifts timing of European floods. Science 357, 588–590.

Chen, L., Chen, X., Cheng, L., Zhou, P., Liu, Z., 2019. Compound hot droughts over china: identification, risk patterns and variations. Atmos. Res. 227 (10), 210–219.

Chen, T., Xia, G., Liu, T., Chen, W., Chi, D., 2016. Assessment of drought impact on main cereal crops using a standardized precipitation evapotranspiration index in Liaoning Province, China. Sustainability 8 (10), 1069.
Coles, S., 2001. An introduction to statistical modeling of extreme values. Springer, New York, NY, pp. 1–208.
Dong, L.Q., Ren, J.H., 1996. The low- and mid-latitude circulation characteristics and moisture transfer during the rainstorms period in the middle reaches of the Huanghe river (in Chinese). Chin. J. Appl. Meteorol. Sci. 7 (2), 160–168.
Fu, G., Charles, S.P., Viney, N., Chen, S., Wu, J.Q., 2007. Impacts of climate variability on stream-flow in the Yellow River. Hydrol. Process. 21 (25), 3431–3439.
Gallant, A.J.E., Karoly, D.J., Gleason, K.L., 2014. Consistent trends in a modified climate extremes index in the United States, Europe, and Australia. J. Clim. 27 (4), 1379–1394.
Gao, X., Zhao, Q., Zhao, X., Wu, P., Pan, W., Gao, X., Sun, M., 2017. Temporal and spatial evolution of the standardized precipitation evapotranspiration index (SPEI) in the loess plateau under climate change from 2001 to 2050. Sci. Total Environ. 595, 191–200.
Gu, L., Chen, J., Yin, J., Xu, C.Y., Chen, H., 2020. Drought hazard transferability from meteorological to hydrological propagation. J. Hydrol. 585, 124761.
Gu, X., Zhang, Q., Li, J., Singh, V.P., Sun, P., 2019. Impact of urbanization on non-stationarity of annual and seasonal precipitation extremes in China. J. Hydrol. 575, 638–655.
Guerreiro, S.B., Dawson, R.J., Kilsby, C., Lewis, E., Ford, A., 2018. Future heat-waves, droughts and floods in 571 European cities. Environ. Res. Lett. 13 (3), 034009.
Hao, Z., Hao, F., Singh, V.P., Ouyang, W., 2017. Quantitative risk assessment of the effects of drought on extreme temperature in eastern China. J. Geophys. Res. Atmos. 122, 9050–9059.
Hao, Z., Hao, F., Singh, V.P., Zhang, X., 2019. Statistical prediction of the severity of compound dry-hot events based on El Niño-Southern Oscillation. J. Hydrol. 572, 243–250.
Hao, Z., Hao, F., Singh, V.P., Ouyang, W., Zhang, S., 2020. A joint extreme index for compound droughts and hot extremes. Theor. Appl. Climatol. 142 (1), 321–328.
Ji, L., Duan, K., 2020. Variations of extreme temperature and its response on regional warming in the Weihe River Basin during 1960–2017 (in Chinese). Sci. Geogr. Sin. 40 (3), 466–477.
Jiang, C., Xiong, L., Xu, C.Y., Guo, S., 2015. Bivariate frequency analysis of nonstationary low-flow series based on the time-varying copula. Hydrol. Process. 29, 1521–1534.
Kundzewicz, Z.W., Pińskwar, I., Brakenridge, G.R., 2018. Changes in river flood hazard in europe: a review. Hydrol. Res. 49, 294–302.
Leonard, M., Westra, S., Phatak, A., Lambert, M., van den Hurk, B., Mclnnes, K., Risbey, J., Schuster, S., Jakob, D., Smith, M.S., 2014. A compound event framework for understanding extreme impacts. Wiley Interdiscip. Rev. Clim. Chang. 5 (1), 113–128.
Li, B.F., Chen, Y.N., Chen, Z.S., Xiong, H., Lian, L., 2016. Why does precipitation in northwest China show a significant increasing trend from 1960 to 2010. Atmos. Res. 167, 275–284.
Li, J.Z., Wang, Y.X., Li, S.F., Hu, R., 2015. A Nonstationary StandardizedPrecipitation Index incorporating climate indices as covariates. J. Geophys. Res. Atmos. 120, 12082–12095.
Li, J., Wang, Z., Wu, X., Zscheischler, J., Chen, X., 2021. A standardized index for assessing sub-monthly compound dry and hot conditions with application in China. Hydrol. Earth Syst. Sci. 25 (3), 1587–1601.
Liu, J., Zhang, Q., Singh, V.P., Gu, X., Shi, P., 2017. Nonstationarity and clustering of flood characteristics and relations with the climate indices in the Poyang Lake 666 Basin, China. Hydrol. Sci. J./Journal Des Sciences Hydrologiques 62 (11), 1809–1824.
Mazdiyasni, O., AghaKouchak, A., 2015. Substantial increase in concurrent droughts and heatwaves in the United States. Proceedings of the National Academy of Sciences of the United States of America, 112 (37), 11484–11489.
McKee, T.B., Doesken, N.J., Kleist, J., 1993. The relationship of drought frequency and duration to time scales. American Meteorological Society, Boston, 8th Conf. on Applied Climatology.
Meng, Q., Bai, H., Sarukkalige, R., Fu, G., Jia, W., Zhang, C., 2021. Annual and seasonal precipitation trends and their attributions in the Qinling Mountains, a climate transitional zone in China. Theor. Appl. Climatol. 144, 401–413.
Miao, C., Sun, Q., Kong, D., Duan, Q., 2016. Record-breaking heat in northwest china in July 2015: analysis of the severity and underlying causes. Bull. Am. Meteorol. Soc. 97 (12), S97–S101.
Milly, P., Betancourt, J., Falkenmark, M., Hirsch, R., Kundzewicz, Z., Lettenmaier, D., Stouffer, R., 2008. Climate change—Stationarity is dead: Whither water management? Science 319, 573–574.
Miralles, D.G., Gentine, P., Seneviratne, S.I., Teuling, A.J., 2019. Land–atmospheric feedbacks during droughts and heatwaves: State of the science and current challenges. Ann. N. Y. Acad. Sci. 1436, 19–35.
Moy, C.M., Seltzer, G.O., Rodbell, D.T., Anderson, D.M., 2002. Variability of El Nino/southern oscillation activity at millennial timescales during the Holocene epoch. Nature 420, 162–165.
Park, J., Sung, J.H., Lim, Y., Kang, H., 2019. Introduction and application of nonstationary standardized precipitation index considering probability distribution function and return period. Theor. Appl. Climatol. 136 (1–2), 529–542.
Parsons, D.J., Rey, D., Tanguy, M., Holman, I.P., 2019. Regional variations in the link between drought indices and reported agricultural impacts of drought. Agr. Syst. 173, 119–129.
Pei, W., Fu, Q., Liu, D., Li, T., 2019. A drought index for rainfed agriculture: the standardized precipitation crop evapotranspiration index (spcei). Hydrol. Process. 33 (5), 803–815.
Peng, S., Ding, Y., Liu, W., Li, Z., 2019. 1 km monthly temperature and precipitation dataset for China from 1901 to 2017. Earth Syst. Sci. Data 11, 1931–1946.
Potop, V., Mozny, M., Soukup, J., 2012. Drought evolution at various time scales in the lowland regions and their impact on vegetable crops in the Czech Republic. Agric. For. Meteorol. 156, 121–133.
Razmi, A., Golian, S., Zahmatkesh, Z., 2017. Non-stationary frequency analysis of extreme water level: application of annual maximum series and peak-over threshold approaches. Water Resour. Manag. 31 (7), 2065–2083.
Ribeiro, A.F.S., Russo, A., Gouveia, C.M., Pires, C.A.L., 2020. Drought-related hot summers: a joint probability analysis in the iberian peninsula - sciencedirect. Weather Clim. Extremes 30, 100279.
Rosner, A., Vogel, R.M., Kirshen, P.H., 2014. A risk-based approach to flood management decisions in a nonstationary world. Water Resour. Res. 50, 1928–1942.
Russo, S., Dosio, A., Sterl, A., Barbosa, P., Vogt, J., 2013. Projection of occurrence of extreme dry-wet years and seasons in Europe with stationary and nonstationary Standardized Precipitation Indices. J. Geophys. Res. Atmos. 118 (14), 7628–7639.
Salas, J.D., Obeysekera, J., 2014. Revisiting the concepts of return period and risk for nonstationary hydrologic extreme events. J. Hydrol. Eng. 19 (3), 554–568.
Salvadori, G., De Michele, C., 2004. Frequency analysis via copulas: theoretical aspects and applications to hydrological events. Water Resour. Res. 40 (12), 229–244.
Salvadori, G., Durante, F., De Michele, C., 2013. Multivariate return period calculation via survival functions. Water Resour. Res. 49 (4), 2308–2311.
Sarhadi, A., Soulis, E.D., 2017. Time-varying extreme rainfall intensity-duration-frequency curves in a changing climate. Geophys. Res. Lett. 44, 2454–2463.
Sarhadi, A., Burn, D.H., Ausin, M.C., Wiper, M.P., 2016. Time-varying nonstationary multivariate risk analysis using a dynamic Bayesian copula. Water Resour. Res. 52, 2327–2349.
Serinaldi, F., Kilsby, C., 2015. Stationarity is undead: uncertainty dominates the distribution of extremes. Adv. Water Resour. 77, 0309–1708.
Shiau, J.T., 2006. Fitting drought duration and severity with two-dimensional copulas. Water Resour. Manage. 20 (5), 795–815.
Song, Z., Xia, J., She, D., Zhang, L., Zhao, L., 2020. The development of a nonstationary standardized precipitation index using climate covariates: a case study in the middle and lower reaches of Yangtze River Basin, China. J. Hydrol. 588 (3), 125115.
Su, C., Chen, X., 2019. Assessing the effects of reservoirs on extreme flows using non-stationary flood frequency models with the modified reservoir index as a covariate. Adv. Water Resour. 124, 29–40.
Um, M.J., Kim, Y., Park, D., Kim, J., 2017. Effects of different reference periods on drought index (spei) estimations from 1901 to 2014. Hydrol. Earth Syst. Sci. 21 (10), 4989–5007.
Van de Vyver, H., Van den Bergh, J., 2018. The Gaussian copula model for the joint deficit index for droughts. J. Hydrol. 561, 987–999.
Vasiliades, L., Galiatsatou, P., Loukas, A., 2015. Nonstationary frequency analysis of annual maximum rainfall using climate covariates. Water Resour. Manag. 29 (2), 339–358.
Vicente-Serrano, S.M., Beguería, S., López-Moreno, J.I., 2010. A multiscalar drought index sensitive to global warming: the Standardized PrecipitationEvapotranspiration Index. J. Clim. 23, 1696–1718.
Villarini, G., Smith, J.A., Serinaldi, F., Bales, J., Bates, P.D., Krajewski, W.F., 2009. Flood frequency analysis for nonstationary annual peak records in an urban drainage basin. Adv. Water Resour. 32 (8), 1255–1266.
Wang, J., Chen, Y., Tett, S.F.B., Yan, Z., Xia, J., 2020. Anthropogenically-driven increases in the risks of summertime compound hot extremes. Nat. Commun. 11 (1), 528.
Wang, R., Guo, L.v., Ning, L., Yuan, L., Li, L., 2021. Likelihood of compound dry and hot extremes increased with stronger dependence during warm seasons. Atmos. Res.
Wang, Y.X., Li, J.Z., Feng, P., Chen, F.L., 2015. Effects of large-scale climate patterns and human activities on hydrological drought: a case study in the Luanhe River basin, China. Natural Hazards 76 (3), 1687–1710.
Wang, Y., Quan, Q., Shen, B., 2019. Spatio-temporal variability of drought and effect of large scale climate in the source region of Yellow River. Geomat. Nat. Haz. Risk 10 (1), 678–698.
Wang, H.J., Yang, Z.S., Saito, Y., Liu, J.P., Sun, X.X., 2006. Interannual and seasonal variation of the Huanghe (Yellow River) water discharge over the past 50 years: connections to impacts from ENSO events and dams. Global Planet. Change 50, 212–225.
Wu, X., Hao, Z., Hao, F., Singh, V.P., Zhang, X., 2019. Dry-hot magnitude index: a joint indicator for compound event analysis. Environ. Res. Lett. 14 (6).
Wu, X., Hao, Z., Zhang, X., Li, C., Hao, F., 2020. Evaluation of severity changes of compound dry and hot events in china based on a multivariate multi-index approach. J. Hydrol. 583, 124580.
Xiong, L., Jiang, C., Xu, C.Y., Yu, K.X., Guo, S., 2015. A framework of changepoint detection for multivariate hydrological series. Water Resour. Res. 51, 8198–8217.
Xu, P., Wang, D., Singh,V.P., Lu, H., Wang, Y., Wu, J., Wang, L., Liu, J., Zhang, J., 2020a. Multivariate hazard assessment for nonstationary seasonal flood extremes considering climate change. Journal of Geophysical Research: Atmosphere, 125(18), e2020JD032780.
Xu, P., Wang, D., Singh, V.P., Lu, H., Wang, Y., Wu, J., Wang, L., Liu, J., Zhang, J., 2020b. Copula-based seasonal rainfall simulation considering nonstationarity. J. Hydrol. 125439.
Yan, L., Xiong, L., Guo, S., Xu, C.-Y., Xia, J., Du, T., 2017. Comparison of four nonstationary hydrologic design methods for changing environment. J. Hydrol. 551, 132–150.
Yilmaz, A.G., Imteaz, M.A., Perera, J.C., 2017. Investigation of non-stationarity of extreme rainfalls and spatial variability of rainfall intensity–frequency–duration relationships: a case study of victoria, australia. Int. J. Climatol. 37, 430–442.

Yu, M., Li, Q., Hayes, M.J., Svoboda, M.D., Heim, R.R., 2014. Are droughts becoming more frequent or severe in China based on the Standardized Precipitation Evapotranspiration Index: 1951–2010? Int. J. Climatol. 34 (3), 545–558.
Zeng, H., Sun, X., Lall, U., Feng, P., 2017. Nonstationary extreme flood/rainfall frequency analysis informed by large-scale oceanic fields for Xidayang Reservoir in North China. Int. J. Climatol. 37 (10), 3810–3820.
Zhang, Y., You, Q., Mao, G., Chen, C., Ye, Z., 2019. Short-term concurrent drought and heatwave frequency with 1.5 and 2.0 ℃ global warming in humid subtropical basins: a case study in the Gan River Basin. China. Climate Dynamics 52, 4621–4641.
Zscheischler, J., Seneviratne, S.I., 2017. Dependence of drivers affects risks associated with compound events. Sci. Adv. 3, e1700263.
Zscheischler, J., Westra, S., van den Hurk, B.J.J.M., Seneviratne, S.I., Ward, P.J., Pitman, A., AghaKouchak, A., Bresch, D.N., Leonard, M., Wahl, T., Zhang, X., 2018. Future climate risk from compound events. Nat. Clim. Chang. 8, 469–477.